Evidence in Earth Science

RESEARCH ARTICLE

DOI: 10.63221/eies.v1i01.52-72

Highlights:

- Feature selection based on the Pearson coefficient can improve the overall accuracy.
- Adding texture & polarization features boosts the OA of the heading and full period.
- The optimal work during milk stage uses optimized texture and polarization features

Keywords:

Sentinel
Feature Selection
Random Forest
Google Earth Engine

Correspondence to:

czc@hpu.edu.cn

Citation: Sun et al., 2025. Extraction of winter wheat planting area across multiple phenological periods based on feature optimization using Sentinel-1/2 data. Evidence in Earth Science, 1(01), 52-72.

Manuscript Timeline

Received	March 21, 2025
Revised	April 3, 2025
Accepted	April 9, 2025
Published	April 15, 2025

Academic Editor:

Yaning Yi

Extraction of winter wheat planting area across multiple phenological periods based on feature optimization using Sentinel-1/2 data

Wenzhi Zhang [1,2,3], Xiaoyu Sun [1], Zhichao Chen [1,2,3,*], Xiaofang Ren [1] and Xiaoyu Li [1]

[1] School of Surveying and Land Information Engineering, Henan Polytechnic University, Jiaozuo, 454000, China

[2] Collaborative Innovation Center of Geo-Information Technology for Smart Central Plains, Zhengzhou, 450052, China

[3] Key Laboratory of Spatiotemporal Perception and Intelligent Processing, Ministry of Natural Resources, Zhengzhou, 450052, China

Abstract Winter wheat constitutes a fundamental cereal crop in China's agricultural system, playing a pivotal role in national food security. Timely and accurate acquisition of winter wheat cultivation area distribution is crucial for effective management, yield estimation, and ensuring food security. This study focuses on Hebi City as the research area, selecting Sentinel-1 and Sentinel-2 imageries from October 2021 to June 2022. The research was conducted on the Google Earth Engine (GEE) cloud computing platform, employing a multi-feature approach that integrated polarization characteristics, spectral properties, vegetation indices, textural features, and topographic parameters across various phenological stages of winter wheat. The random forest algorithm was implemented for crop classification and area extraction. The results show that: (1) The optimized feature sets constructed based on the Pearson correlation coefficient can improve overall classification accuracy, with an overall accuracy exceeding 90% across all schemes. (2) Adding both texture and polarization features can improve the overall classification accuracy of the heading stage and the full phenological period, most significantly in the full phenological period; (3) The extraction scheme for winter wheat planting area during the milk ripening stage, considering the optimized texture features and preferred polarization features, is the most effective method, achieving an overall accuracy of 98.1% and a Kappa coefficient of 0.976. The achievements of this research have broad application prospects in guiding regional precision winter wheat cultivation, optimizing agricultural resource allocation, supporting grain yield prediction, and ensuring national food security. It is expected to provide strong data support and technical references for agricultural management departments in making scientific decisions.

1. Introduction

As a crucial staple crop in China's agricultural system, winter wheat exhibits substantial interannual variability in its cultivated acreage. Precise and timely monitoring of the spatial distribution patterns and cultivation extent of this crop enables

agricultural management agencies to make data-driven decisions and implement effective agricultural policies. The accurate delineation of winter wheat planting areas serves as a fundamental basis for yield forecasting, resource allocation, and sustainable agricultural planning (Tian et al., 2022). Traditional methods of monitoring agricultural planting areas are inefficient and often lack comprehensive coverage. In addition, they can be significantly influenced by subjective factors of surveyors (Wang et al., 2023). Remote sensing technology provides substantial benefits in acquiring data on the distribution of crop planting areas, characterized by extensive coverage, promptness, and cost-effectiveness. As a result, it has been widely applied in agricultural production (Huang et al., 2022).

The current studies on the extraction of winter wheat planting area using satellite remote sensing can be categorized into three main aspects. The first aspect is the data sources utilized in the research, which can be divided into single data source and multi-source data. The second aspect pertains to the phenological period, which includes single phenological period and multi-phenological period. The third aspect is the feature set, which can be either single feature or multi-feature set. From the perspective of data sources, most studies use a single remote sensing sensor such as sentinel-1 (Wang et al., 2024; Xiao et al., 2023; Schlund and Erasmi, 2020), sentinel-2 (Wang et al., 2023; Chen et al., 2024; Liu et al., 2024; Mashonganyika et al., 2021), MODIS (Potgieter et al., 2007; Ren et al., 2021), and Landsat (Zhang et al., 2023) to extract the winter wheat planting area. Passive optical remote sensing is the main data source that is used in the current crop classification research. Active radar remote sensing is distinguished by the capability to acquire all-weather data continuously and its significant penetrating ability (Lucas et al., 2020). Active and passive remote sensing have their own advantages, but land cover information reflected by a single sensor is limited. The integration of multi-source data significantly enhances the precision of delineating winter wheat planting areas (Li et al., 2023; Ma et al., 2021; Zhang et al., 2023; Zhang et al., 2019; Blickensdörfer et al., 2022).

As for any specific phenological time for research and experiments, experts and scholars usually extract the winter wheat planting area based on one or several images within the phenological period (Luo et al., 2019; Zhao et al., 2022; Yang et al., 2020; Liu et al., 2022; Qu et al., 2021), which seems efficient and operable. However, when the planting structure in the study area is complex and identifying "crop's key phenological characteristics" becomes challenging, the results and accuracy obtained by using this method are often not satisfactory (Hu et al., 2015). The extraction of winter wheat planting information by integrating multiple or even full phenological periods (Li et al., 2019; Wu et al., 2023; Sun et al., 2024) makes full use of spectral and spatial characteristics, and takes into account the changes of characteristic indices during the whole growth cycle, which can avoid the impacts of some external factors such as sudden weather changes and man-made destruction.

In terms of the application of feature sets in classification and recognition, the commonly used features used for extracting winter wheat planting information based on a single feature are NDVI (Qi et al., 2022; Jakubauskas et al., 2002; Atzberger and Rembold, 2013; Li et al., 2021) and EVI (Yan et al., 2009; Pan et al., 2011; Zhao et al., 2021), while the multi-feature set is mostly composed of spectral features, vegetation index features, texture features, terrain features, and polarization features (Chang et al., 20245; Xie et al., 2024; Zhang et al., 2023). The technique for extracting the cultivated area of winter wheat using a singular characteristic from time-series images is highly practical and efficient; however, the choice of a single characteristic is significantly subjective. The integration of multi-dimensional characteristic quantities can effectively solve the problems of spectral mixing or variation at the junction and inside of mixed crops. This method is also suitable for the regions with complex crop planting structures (Hu et al., 2015).

Although using multiple feature sets can improve winter wheat identification accuracy, too many features may cause data redundancy. This negatively affects classification efficiency and accuracy. Therefore, how to scientifically select features and reduce dimensionality has become an urgent problem to solve. At present, although some researches have explored the method of feature selection, the comprehensive and systematic feature selection based on the fusion of sentinel active

and passive remote sensing data, combined with a variety of features, and at the same time, the research on the influence of phenology and feature index on the extraction accuracy of winter wheat is still insufficient.

Thus, feature dimensionality reduction becomes essential. Feature optimization serves as a dimensionality reduction technique. It involves selecting a subset of features from the original set based on specific criteria (Cai et al., 2018). Some scholars optimized the characteristics according to the importance of random forest characteristics (Amini et al., 2022). Other scholars have extracted winter wheat based on the combination of random forest parsimony feature and Pearson correlation coefficient, and proved that this method can improve the classification accuracy and the efficiency of classifier (Feng et al., 2022). It provides a feasible basis for the feature optimization method based on Pearson correlation analysis.

To sum up, this study uses the fusion of sentinel active and passive remote sensing data as the data source, and comprehensively uses spectral features, vegetation index features, terrain features, texture features and polarization features, and carries out feature optimization. By setting different classification schemes, the aim is to improve the accuracy of winter wheat planting area extraction, and to explore the impact of phenology and characteristic index on the extraction accuracy, so as to explore the optimal scheme of winter wheat planting area extraction, make up for the shortcomings of existing research, and provide more efficient and accurate technical methods for winter wheat planting monitoring.

2. Data and Methods

2.1. Study Area

Hebi City, an important winter wheat planting area, is located in the north of Henan Province, spanning from 35°26′0″ to 36°2′54″ north latitudes and from 113°5′23″ to 114°45′12″ east longitudes (Figure 1). Hebi City is situated at the confluence of the eastern Taihang Mountains and the North China Plain, spanning a total area of 2,182 square kilometers. The topography of Hebi City is characterized by mountains in the northwest, hills extending in a north-south direction across the central and eastern parts, and plains in the eastern and southeastern areas. The region experiences a warm temperate semi-humid monsoon climate, with an annual average temperature ranging from 14.2 to 15.5 ℃, annual precipitation between 349.2 and 970.1 mm, and annual sunshine duration from 1,787.2 to 2,566.7 hours. The agricultural system in this area is based on a winter wheat-summer maize rotation. Winter wheat is typically sown in mid-October and harvested in early June of the following year.

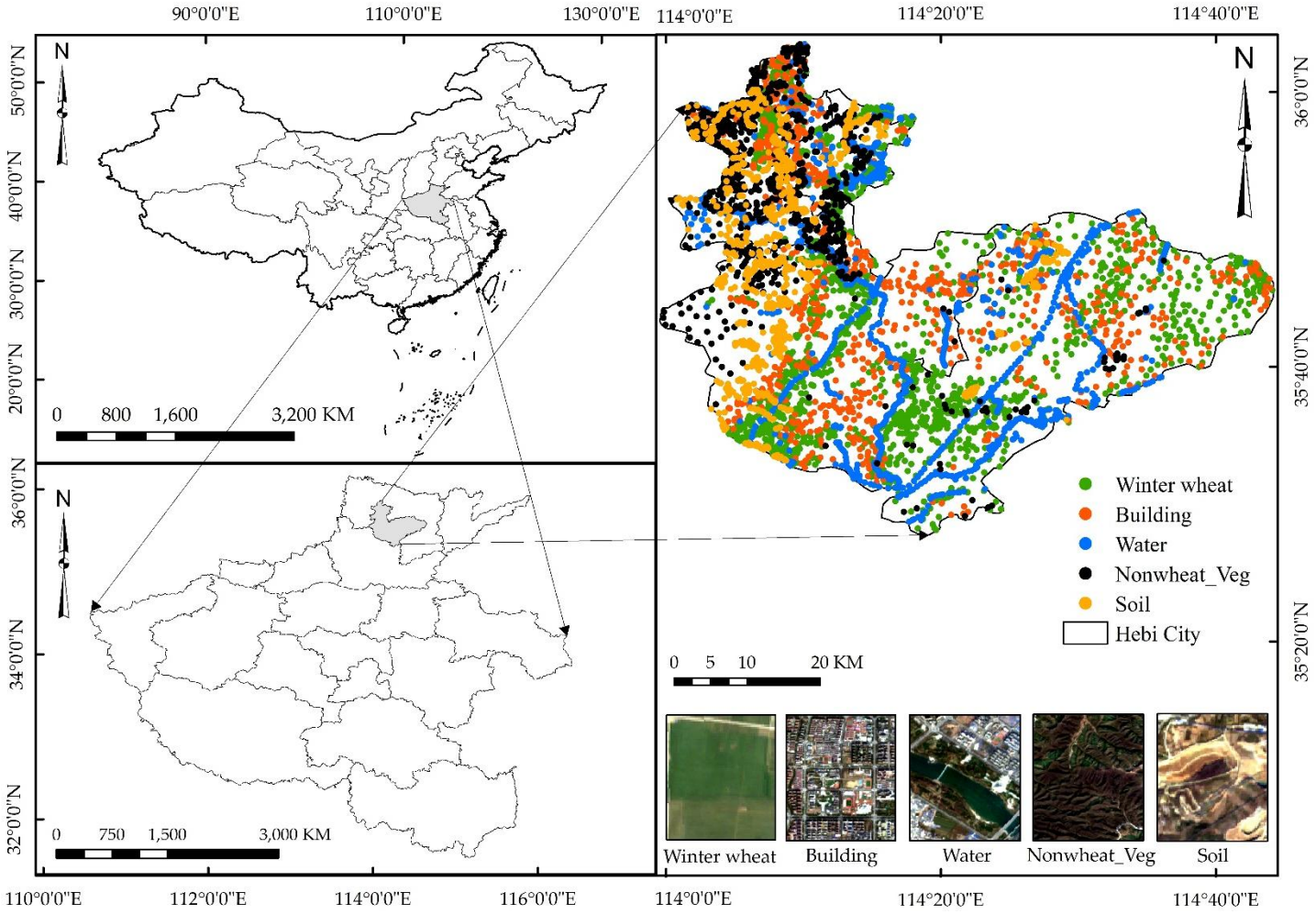

Fig. 1 The location of Hebi City and the distribution map of sample points

2.2. Data

2.2.1. Sentinel Image

The high spatial-temporal resolution and unrestricted access to sentinel data have made it highly favored among agricultural remote sensing specialists and scholars, establishing it as the primary data source for crop remote sensing monitoring. The download and processing of sentinel active and passive remote sensing data in this study are based on the GEE (Google Earth Engine) platform, and the required remote sensing data can be called through "ee.imagecollection("COPERNICUS/S1_GRD"), " ee.imagecollection("COPERNICUS/S2_SR_HARMONIZED").

In this study, we selected sentinel-1 interference wideband (IW) mode imaging, including 10m resolution GRD products with VV and VH polarization modes. For the sentinel-1 GRD product data, firstly, the terrain correction algorithm built in the GEE platform is used, combined with the digital elevation model (DEM) data of the study area, to correct the terrain, so as to eliminate the influence of terrain fluctuation on the radar backscatter coefficient. After correction, S-G filtering algorithm is used for filtering and noise reduction. After the above processing, 10m resolution images including VV and VH polarization modes are obtained.

Sentinel-2 adopts L2A product after atmospheric correction. Firstly, the data are filtered according to the cloud content less than 20% to reduce the interference of cloud on the image spectral information. We assessed the filtered photos,

discarded data significantly affected by cloud cover, and retained photographs devoid of clouds or with minimal cloud interference. Due to the differences in the original resolution of different bands of sentinel-2, in order to facilitate subsequent analysis, the resolution of all bands of the image is uniformly resampled to 10m through bicubic curve resampling. The elevation data of the study area can be obtained from GEE platform through "ee.image (" usgs/srtmgl1_003 "). The elevation data is added to the sentinel-2 image as a new band.

2.2.2. Sample Data

Given that field sampling is more labor-intensive and material-consuming, this paper selected samples by visual inspection and manual selection based on the Sentinel-2 optical images combined with Google Earth images. Based on the land cover characteristics in the study area, the ground objects were divided into winter wheat (wheat), building land (building), water (water), non-winter wheat vegetation (nonwheat_Veg), and bare soil (soil). Among them, non-winter wheat vegetation included all green vegetation except winter wheat, comprising other crops, shrubs, grasslands, woodlands, etc.; building samples included houses, roads, greenhouses and lands under construction; bare soil samples included bare lands covered with artificial materials such as sand and stones. To ensure the selecting accuracy of winter wheat sample points and using the cloud-free images of the study area during the overwintering period of winter wheat (February 26, 2022), contiguous green areas were selected as winter wheat sample points. Non-winter wheat vegetation samples were selected based on the image of the winter wheat milky-ripe stage (June 16, 2022), and bare soil samples were selected based on the image of the winter wheat heading and flowering stage (May 17, 2022). Finally, 1500 winter wheat samples, 880 built-up area samples, water bodies, and non-winter wheat vegetation, and 860 bare soil samples were selected, making up a total of 5000 sample points. The sample points, distributed as shown in Figure 1, were randomly divided into training and validation samples at a ratio of 7:3.

2.2.3. Statistical Data

The data on winter wheat planting areas in each county and district of Hebi City are sourced from the Henan Statistical Yearbook and the Hebi Statistical Yearbook. These data are utilized to assess the accuracy of winter wheat planting area extraction in Hebi City for the year 2021.

2.3. Methods

On the Google Earth Engine (GEE) platform, Sentinel active and passive remote sensing images of the study area were collected for the entire phenological period of winter wheat from October 1, 2021, to June 30, 2022. These images were used to generate the NDVI variation curve, as depicted in Figure 2.

It can be seen in Figure 2 that during October 24, 2021 to December 28, 2021, the NDVI value of winter wheat gradually increased, while the NDVI value of other green vegetation decreased, and the two intersected, which was considered as the winter wheat seedling stage and tillering stage, respectively. From December 28, 2021 to March 8, 2022, the NDVI value of winter wheat fluctuated but remained unchanged on the whole, which should be the overwintering period of winter wheat. During this period, the NDVI value of other non-winter wheat vegetation gradually decreased. From March 8, 2022 to April 2, 2022, winter wheat was in the reviving stage, and the NDVI value increased rapidly. At this time, the majority of the other vegetation covers have not yet verdantly emerged and flourished, and the gap between the NDVI value of winter wheat and other vegetation began to increase. April 2, 2022 to May 2, 2022, was considered the jointing and booting stage of winter wheat (hereinafter referred to as the jointing stage). At this time, organs such as ears, leaves and stems grew simultaneously, the leaf area and the length and volume of stems and ears increased by several or dozens of times, and the accumulation of dry matter also entered a rapid growth stage. At this time, the difference in NDVI value between winter wheat and other vegetation classes was largest. By early May, winter wheat entered the heading and flowering stage (hereinafter referred to as the heading stage). The nutrients in the wheat plants were transported to the grains in the ears and accumulated, and the grains began to deposit starch. In June, upon reaching the milky-ripe stage, the wheat grains yellowed and the plants desiccated, resulting in a rapid decline of the NDVI value for

winter wheat, which fell below the NDVI characteristic value of other vegetation types and intersected with their NDVI curve.

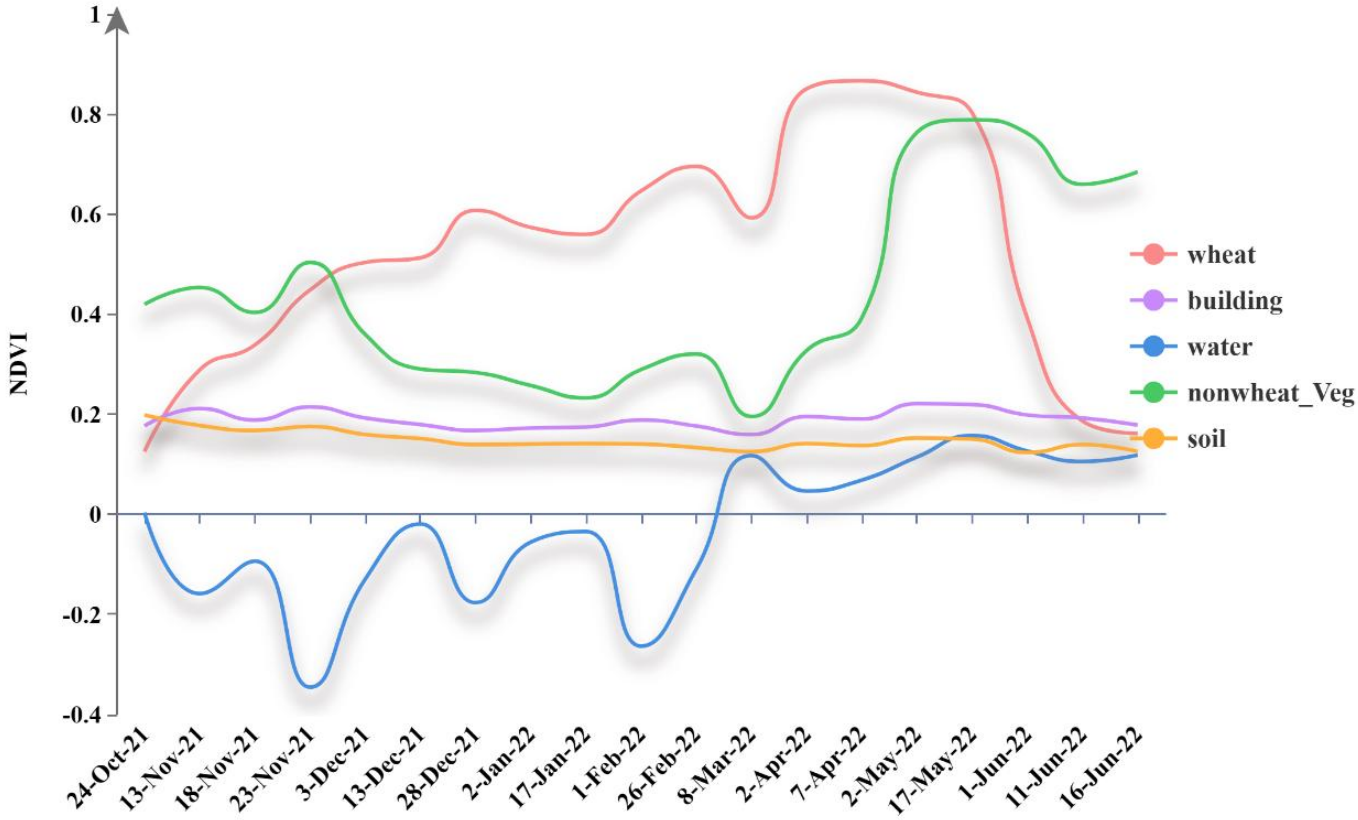

Fig. 2 NDVI Changes in different land features

Thus, the whole phenological period of winter wheat was divided into six phenological periods: seedling stage, overwintering stage, reviving stage, jointing stage, heading stage, and milky-ripe stage (Table 1). In terms of time, the mean values of the filtered images were synthesized into one image corresponding to the phenological period, resulting in a total of 6 Sentinel-2 images. The multi-band images of each phenological period were subjected to Pearson correlation analysis for feature selection. Based on the optimized feature variables, the random forest algorithm was used to extract winter wheat, and the contribution of different feature variables to the extraction of winter wheat and the influence of different phenological periods on the identification and extraction of winter wheat were explored.

Table 1. Key phenological calendar and image number

Phenological period	*Time frame*	*Number of images*
Seedling stage	2021.10.24-2021.12.30	6
Overwintering stage	2022.01.01-2022.03.09	5
Reviving stage	2022.03.10-2022.04.03	3
Jointing stage	2022.04.04-2022.05.03	2
Heading period	2022.05.04-2022.06.01	1
Milk ripening period	2022.06.01-2022.06.30	3

2.3.1. Feature Set Construction

In remote sensing classification, feature selection is crucial. Properly chosen features can significantly enhance classification accuracy (Luo et al., 2022). This paper identifies 12 spectral characteristics, 10 associated vegetation index characteristics, terrain characteristics, and texture characteristics from Sentinel-2 image data, based on the phenological attributes of ground objects and the crop planting structure in the study area. It also incorporates the polarization characteristics of Sentinel-1, along with addition, subtraction operations, and ratio polarization characteristics of the two, to construct the feature set, as detailed in Table 2.

Table 2. Characteristic variables

Satellite	*Group*	*Characteristic variables*
Sentinel-1	Polarization features	VV
		VH
		ratio = VV/VH
		plus = VV+VH
		reduce = VV-VH
Sentinel-2	Index features	Normalized Difference Vegetation Index (NDVI) (RouseJr et al.,1973)
		Green Normalized Difference Vegetation Index (GNDVI) (Gitelson et al., 1996)
		Enhanced vegetation index (EVI) (Huete et al., 1997)
		Optimized Soil-Adjusted Vegetation Index (OSAVI) (Rondeaux et al., 1996)
		Modified Soil Adjusted Vegetation Index (MSAVI) (Qi et al., 1994)
		Modified Normalized Difference Water Index (MNDWI) (Xu., 2005)
		Normalized Difference Building Index (NDBI) (Zha et al., 2003)
		Bare soil index (BSI) (Diek et al., 2017)
		Modified Bare soil index (MBI) (Nguyen et al., 2021)
		Enhanced Modified Bare Soil Index (EMBI) (Zhao and Zhu., 2022)
	Spectral features	Full spectrum bands
	Topographic features	Elevation
		Slope
	Texture features	Angular Second Moment (ASM)
		Contrast
		Correlation
		Variance
		Inverse Differential Moment (IDM)
		Entropy
		Mean
		Dissimilarity

Spectral characteristics serve as the fundamental basis for judging and classifying the types of various features in remote sensing images. All bands of Sentinel-2 images were selected as spectral band features. Vegetation index features were calculated from the combination of different bands, and hence each index has different advantages and functions in classification. Based on the literature and the spectral characteristics of winter wheat, ten vegetation indices were selected (Radočaj et al., 2023), including Enhanced Vegetation Index (EVI), Normalized Vegetation Index (NDVI), Green Normalized Difference Vegetation Index (GNDVI), Optimizing soil adjusted vegetation index (OSAVI), Modified soil adjusted vegetation index (MSAVI), Modified Normalized Difference Water Index (MNDWI), Normalized difference building index (NDBI), Bare soil index (BSI), Modified Bare Soil Index (MBI), Enhanced modified bare soil index (EMBI).

Texture features were extracted from images using the Gray-level Co-occurrence Matrix (GLCM) method. These features are essential for identifying surface characteristics in images, since different surface features exhibit unique texture patterns. Some researchers believe that adding texture features can effectively improve the phenomenon of "same object with different spectra, different objects with the same spectra" (Xiong et al., 2021). The GLCM takes the gray level and position of the pixel as the research object, reflecting multi-dimensional information such as the direction, adjacent interval, and variation amplitude of the pixel's gray level (Liu et al., 2022). In GEE, the "glcmTexture()" function can be used to calculate GLCM texture features.

To avoid the redundancy caused by too many texture features in the process of training classification models, eight most commonly used texture features were selected, including angular second moment, contrast, correlation, variance, mean, dis-similarity, inverse difference moment, and entropy.

2.3.2. Random Forest Algorithm

The random forest (RF) algorithm was chosen for classification. RF consists of multiple CART decision trees and belongs to the supervised classification machine learning algorithms. Relevant research shows that RF algorithm has good classification accuracy and robustness compared with other machine learning algorithms (Pu et al., 2020; Yao et al., 2022). The RF algorithm in GEE can also determine the weight of input features at the same time, which is widely used in remote sensing supervised classification (Praticò et al., 2021). RF algorithm requires two variables: the number of feature variables and the number of decision trees. The number of feature variables is mostly fixed, while the number of decision trees needs to be determined. The classification accuracy diminishes with an insufficient number of decision trees, while an excessive quantity leads to stabilized accuracy at the expense of operational speed. The GEE platform can perform hyperparameter tuning for the number of decision trees. When the number of decision trees is greater than 50, the classifier accuracy basically remains stable (Guo et al., 2021). Therefore, during classification, hyperparameter tuning tests are performed within the range of 0-50 for the number of decision trees. We tried a series of values and selected the minimum value likely to produce the highest accuracy. This allowed us to extract winter wheat with the best classification accuracy by selecting the optimal number of decision trees.

2.3.3. Feature Optimization

The total number of features selected in the early stage was 35, which made full use of the spectral and spatial information of the image. Nevertheless, an increased number of features did not correlate with enhanced quality. Excessive features will not only increase the complexity of the model and information redundancy, but can also cause "dimensional disaster", thereby reducing the classification performance (Uddin et al., 2021). This study utilizes the Pearson correlation coefficient to examine all classification features and variable types. Features with an absolute correlation coefficient greater than 0.8 are removed to reduce model redundancy.

Pearson correlation coefficient quantifies the linear relationship between two variables by calculating the quotient of the covariance and the product of standard deviations of the two variables. Its value ranges from -1 to 1, with 1 indicating a perfect positive correlation, -1 indicating a perfect negative correlation, and 0 indicating no linear relationship. According to the absolute value of the correlation coefficient, the strength of linear correlation is divided into: 0.00-0.19

"very weak", 0.20-0.39 "weak", 0.40-0.59 "medium", 0.60-0.79 "strong", and 0.80-1.00 "very strong". Correlation coefficient can be expressed as follows:

$$r = \frac{\sum\left(X_i - \overline{X}\right)\left(Y_i - \overline{Y}\right)}{\sqrt{\sum\left(X_i - \overline{X}\right)^2 \left(Y_i - \overline{Y}\right)^2}} \quad (1)$$

Where, (r) represents the Pearson correlation coefficient, which reflects the degree of linear correlation between two variables; (X_i) is the i-th data point of variable X; (Y_i) is the i-th data point of variable Y; ($\overline{X}$)is the mean value of variable X; ($\overline{Y}$)is the mean value of variable Y.

2.3.4. Accuracy Assessment

To effectively evaluate the extraction accuracy of winter wheat areas, four indicators, including Overall Accuracy (OA), Producer Accuracy (PA), User Accuracy (UA), and Kappa coefficient, were selected(Wu et al., 2023). The extracted winter wheat planting area was compared with the winter wheat planting area of Hebi City and its five counties and districts provided by the Henan Statistical Yearbook and the Hebi Statistical Yearbook. The results of classification were assessed using the coefficient of determination (R^2) and the root mean square error (RMSE) of the fitting curve between the two variables.

2.3.5. Experimental Design

In order to explore the ability of the Sentinel's active and passive remote sensing to extract winter wheat, and to compare the effects of different phenological periods and characteristic variables on the winter wheat extraction accuracy, the best plan to achieve the maximum improvement in the accuracy of winter wheat extraction was determined. Based on the optimization of terrain features, spectral features, and vegetation index features, eight classification schemes (Table 3) were designed. Among them, the difference between Schemes 1, 2, 3, and 4 and Schemes 5, 6, 7, and 8 lies in whether the polarization feature is added. Schemes 1, 3, 5, and 7 and Schemes 2, 4, 6, and 8 are compared to study the impact of texture features on classification accuracy. Schemes 1, 2, 5, and 6 and Schemes 3, 4, 7, and 8 were set to explore the impact of the single and full phenological periods on the extraction of winter wheat.

Table 3. Classification Plan

Plan	*1*	*2*	*3*	*4*	*5*	*6*	*7*	*8*
Single phenological period	☑	☑			☑	☑		
Full phenological period			☑	☑			☑	☑
Topographic features	☑	☑	☑	☑	☑	☑	☑	☑
Spectral features	☑	☑	☑	☑	☑	☑	☑	☑
Vegetation index features	☑	☑	☑	☑	☑	☑	☑	☑
Texture features		☑		☑		☑		☑
Polarization features					☑	☑	☑	☑

2.3.6. Technical Route

The technical route of this study is shown in Figure 3. Firstly, the whole growth period of winter wheat is divided into different growth periods according to the NDVI time series change curves of different features. According to the divided

Reviving stage and Heading period, the sample data are selected in combination with Google Earth; Secondly, sentinel image data and SRTM terrain data during the growth period of winter wheat were obtained in GEE platform, and polarization features, spectral features, vegetation index features, texture features and terrain features were extracted respectively; Thirdly, the extracted texture features are analyzed by principal component analysis, and the first three principal components are retained to replace the texture features. The Pearson correlation coefficient is used to analyze the correlation of other features, and the feature quantity with correlation coefficient greater than 0.8 is eliminated to construct the optimal feature set; Finally, different features are set to participate in the extraction of winter wheat planting area, the extraction accuracy of different schemes is analyzed, and the influence of different features on the extraction of area is explored, so as to explore the best extraction scheme for winter wheat in Hebi.

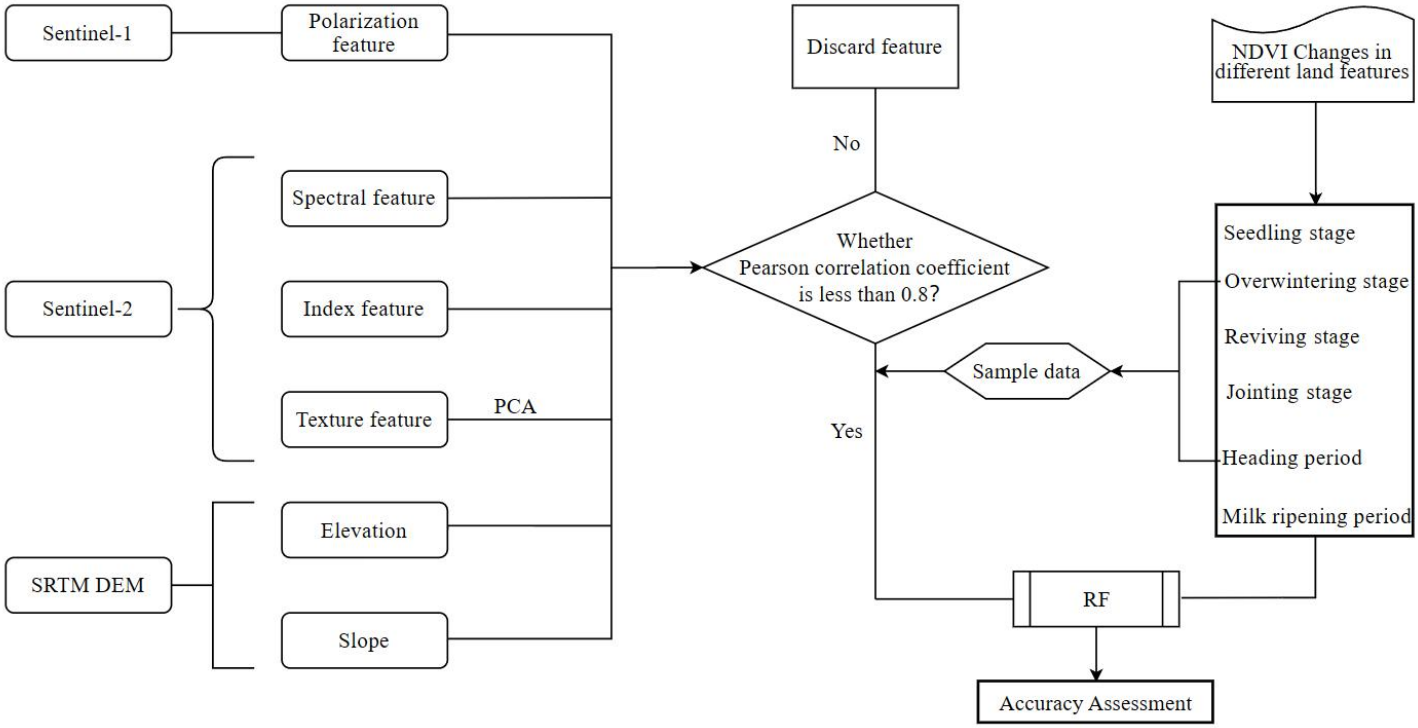

Fig. 3 Technology Roadmap

3. Results

3.1. Preferred Categorical Features

3.1.1. Opting for Topographic, spectral and vegetation index features

Taking the image at seedling stage as an example, the Pearson correlation coefficient matrix is shown in Figure 4. The visible light band is a commonly used band in optical classification and will not be removed. The correlation coefficients between RE1(B5) and Green(B3), Red(B4) were greater than 0.8, so the RE1 band was eliminated. The correlation coefficients between RE2(B6), RE3(B7), Narrow NIR(B8), and Narrow NIR(B8A) were all higher than 0.8. Considering that Narrow NIR(B8) is one of the most widely used bands in spectral characteristic research, B8A band was retained. The correlation coefficients between Water vapor(B9) and SWIR(B11) with B8A was greater than 0.8 for both, so they were eliminated. The correlation coefficients between NDVI, GNDVI and OSAVI were higher than 0.8 for both, so the NDVI feature was eliminated. GNDVI and EMBI had a high correlation with MNDWI, so MNDWI was eliminated. OSAVI had a high correlation with MSAVI, so OSAVI was eliminated. The correlation coefficient between BSI and NDBI was 0.82. Considering the need to extract building areas, the BSI feature band was eliminated. The correlation coefficient between

MBI and NDBI was 0.91, so MBI was eliminated. The correlation coefficient between the height feature (elevation) and slope feature (slope) in topographic features was 0.81. Based on the classification requirements, the slope feature was eliminated. Therefore, the selected features during the seedling stage were B1, B2, B3, B4, B8A, NDBI, GNDVI, EVI, MSAVI, EMBI, and elevation.

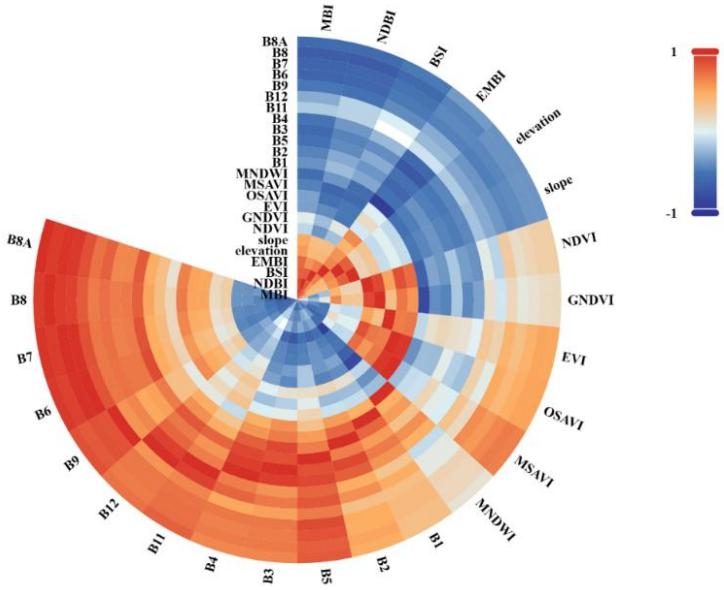

Fig. 4 Pearson correlation coefficient matrix at the seedling stage

3.1.2. Opting for Polarization features

The Pearson correlation analysis of the five feature variables of Sentinel-1 image in seedling stage is shown in Figure 5. It can be seen that the sum of polarization values is highly correlated with VV and VH. In this paper, VV, VH, ratio and reduce are selected as polarization feature variables.

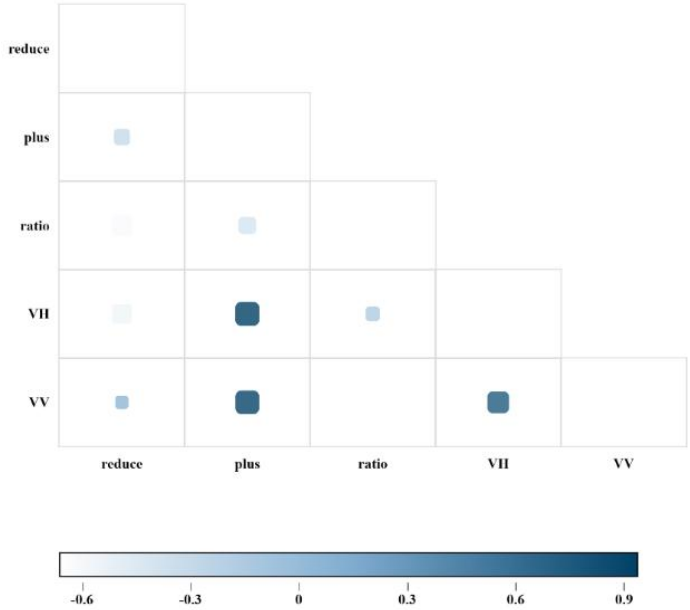

Fig. 5 Correlation coefficient of polarization characteristics at the seedling stage

3.1.3. Opting for Texture features

On the GEE platform, the gray-level co-occurrence matrix is used to extract image texture features, and the results of the PCA analysis of its texture features are shown in Table 4. The first three principal components already contain 99.99% of the information, so the first three principal components of texture features were selected as the optimal feature variables.

Table 4. Principal component analysis results of texture features

Characteristic components	*Percentage (%)*
PC1	93.55
PC2	4.20
PC3	2.24
PC4	0.01
PC5	0.00
PC6	0.00
PC7	0.00
PC8	0.00

For each phenological period, based on the Pearson correlation coefficient among multiple indices of topographic characteristics, spectral characteristics and vegetation index characteristics, the characteristic indices with the absolute value greater than 0.8 were eliminated, and the optimal feature set for each phenological period was generated as shown in Table 5.

Table 5. Optimal feature sets of topographic features, spectral features, and vegetation index features

Phenological period	*Preferred feature set*
seedling stage	B1, B2, B3, B4, B8A, NDBI, GNDVI, EVI, MSAVI, EMBI, elevation
Overwintering period	B1, B2, B3, B4, B8A, B11, NDBI, GNDVI, EVI, EMBI, elevation
Rejuvenation	B2, B3, B4, B8A, MNDWI, EVI, EMBI, elevation
Jointing stage	B2, B3, B4, B6, B8A, MNDWI, EVI, EMBI, elevation
Heading period	B2, B3, B4, B6, B8A, MNDWI, EVI, EMBI, elevation
Milk ripening period	B1, B2, B3, B4, B8A, NDBI, MNDWI, GNDVI, EVI, elevation
Full phenological period	B2, B3, B4, B8A, B11, NDBI, GNDVI, EVI, EMBI, elevation

Using VV, VH, ratio and reduce as the preferred polarization characteristic variables, and the first three principal components of texture features as the preferred texture features, the classification feature set of each phenological period was constructed.

3.2. Comparative analysis of the classification accuracy of different schemes

The GEE platform facilitates the RF classification of Sentinel active and passive remote sensing images of winter wheat throughout its entire phenological period in Hebi City, enabling the extraction of winter wheat planting areas. Additionally, the impact of various feature indices on the extraction accuracy of winter wheat during different phenological stages was examined (Table 6).

Among these, the highest accuracy was achieved in scheme 5 by adding polarization features during the seedling stage, with an overall accuracy of 97.3% and a Kappa coefficient of 0.966. The highest accuracy was achieved in scheme 2 by adding texture features and excluding polarization features during the overwintering stage, with an overall accuracy of 97.2% and a Kappa coefficient of 0.964. The highest classification accuracy was achieved in scheme 1 by excluding both texture and polarization features during the reviving stage, with an overall accuracy of 97.2% and a Kappa coefficient of 0.965, and a winter wheat mapping accuracy of 100%. The highest accuracy was achieved in scheme 5 by adding

polarization and excluding texture features during the jointing stage, with an overall accuracy of 97.5% and a Kappa coefficient of 0.968. The highest classification accuracy was achieved in scheme 6 by adding both polarization and texture features during the heading and milky-ripe stages, with an overall accuracy of 97.8% and a Kappa coefficient of 0.972. During the whole phenological period, the best result was achieved in scheme 7 with only optimal polarization features added, with an overall accuracy of 98.6% and a Kappa coefficient of 0.983, which was also the highest overall accuracy among all schemes.

Table 6. Classification accuracy statistics

Plan	*Index*	*Seedling*	*Overwintering*	*Rejuvenation*	*Jointing*	*Heading*	*Milk ripening*	*Full period*
1,3	OA/%	96.8	93.4	97.2	93.2	93.7	96.8	93.4
	KAPPA	0.959	0.916	0.965	0.914	0.920	0.960	0.916
	UA/%	98.9	98.9	99.6	98.6	98.9	97.6	99.3
	PA/%	99.3	100.0	100.0	98.4	98.9	99.1	99.8
2,4	OA/%	91.8	97.2	93.9	97.5	97.3	97.8	94.9
	KAPPA	0.896	0.964	0.922	0.968	0.965	0.972	0.935
	UA/%	97.1	100.0	99.8	99.4	99.3	98.9	99.8
	PA/%	98.7	100.0	99.8	99.4	99.3	98.9	99.8
5,7	OA/%	97.3	97.0	93.7	97.5	97.5	92.4	98.6
	KAPPA	0.966	0.962	0.920	0.968	0.968	0.904	0.983
	UA/%	99.1	99.8	99.3	99.8	99.8	97.5	99.5
	PA/%	99.3	100.0	99.6	99.8	99.8	97.5	99.5
6,8	OA/%	92.7	93.3	93.7	93.6	97.8	98.1	98.4
	KAPPA	0.907	0.915	0.920	0.918	0.972	0.976	0.980
	UA/%	97.6	99.5	99.3	99.8	100.0	99.1	99.8
	PA/%	99.6	100.0	99.1	98.9	100.0	98.7	100.0

Schemes 2 and 4 added optimal texture features on the basis of Schemes 1 and 3, with an overall classification accuracy improvement of 4.3% during the jointing stage, 3.8% during the overwintering stage, 3.6% during the heading stage, 1.5% for the whole phenological period, and 1% during the milky-ripe stage, and with a reduction of 5% and 3.3% during the seedling stage and reviving stage respectively. Schemes 5 and 7 added optimal polarization features on the basis of Schemes 1 and 3, with an overall accuracy improvement of 5.2% for the whole phenological period, 4.3% during the jointing stage, 3.8% during the heading stage, 3.6% during the overwintering stage, and a slight increase of only 0.5% during the seedling stage, with a reduction of 4.4% and 3.5% during the milky-ripe stage and reviving stage respectively. Schemes 6 and 8 added both optimal polarization and texture features on the basis of Schemes 1 and 3, with the largest overall accuracy improvement of 5% for the whole phenological period, 4.1% during the heading stage, 1.3% during the milky-ripe stage, and only 0.4% during the jointing stage, with a reduction of 4.1%, 3.5%, and 0.1% during the seedling stage, reviving stage, and overwintering stage respectively. It can be concluded that the inclusion of texture features, polarization features, or both separately enhances the overall accuracy during the entire phenological period and heading stage to varying extents, whereas the overall accuracy during the reviving stage diminishes by 3%, irrespective of the addition of texture features, polarization features, or both. By ignoring changes with fluctuations of less than one percent, it can be considered that the optimal polarization features have no effect on extracting winter wheat information during the seedling stage, and adding both types of optimal features simultaneously has no effect on extracting winter wheat information during the overwintering and jointing stages.

This study examines the effects of various phenological stages on the extraction of winter wheat data from distinct feature sets, with the optimal phenological stages for each scheme presented in Table 7. Schemes 1, 2, 5, and 6 are comparative schemes for individual phenological stages. Scheme 6 has the highest overall classification accuracy of 98.1% for the milky ripe stage after adding all features. Schemes 3, 4, 7, and 8 are comparative schemes for the entire phenological stage. When optimal polarization features are selected, Scheme 7, which does not add optimal texture

features, has the best overall classification for the entire phenological stage. The overall classification accuracy of Scheme 8, which adds optimal texture features for the entire phenological stage, is slightly lower, but this difference can be ignored. However, at this time, the producer accuracy of winter wheat is the best.

This paper selects the best classification scheme from scheme 6 of full-feature milk maturity, scheme 7 of full phenological period, and scheme 8 of full-feature full phenological period. The classification results of the three are shown in Figure 6. It is obvious that the biggest difference lies in the identification of land types in the central and eastern regions of the city. In Figure 6a, this area is identified as winter wheat. In Figure 6b, it is divided into water body types, while the central and eastern regions of Hebi are generally residential areas and farmland. Scheme 7 of full phenological period is excluded. In Figure 6c, it is divided into other vegetation types that are not winter wheat.

Table 7. Optimal classification phenological period

Plan	*Optimal classification phenological period*	*Overall Accuracy (%)*
1	Rejuvenation	97.2
2	Milk ripening period	97.8
3	Full phenological period	93.4
4	Full phenological period	94.9
5	Jointing stage	97.5
6	Milk ripening period	98.1
7	Full phenological period	98.6
8	Full phenological period	98.4

Henan Modern Agricultural Big Data Industry Technology Research Institute Co., Ltd. has established a 5G intelligent agricultural industry demonstration base (Figure 6d) in Shiqiao Village, Qiaomeng Town, Qi County, Hebi City. The test area is flat and contiguous, with clay soil type, good irrigation conditions, with the main planting mode of winter wheat and summer corn rotation. To further select the optimal scheme, the classification results of scheme 6 full-feature milky-ripe period and scheme 8 full-feature full phenological period extracted from this experimental field area were studied. In Figure 6f, the winter wheat area that was intended to be red was erroneously segmented into blue water bodies and green non-winter wheat vegetation. Relatively speaking, the misclassification of full-feature milky-ripe period was lower.

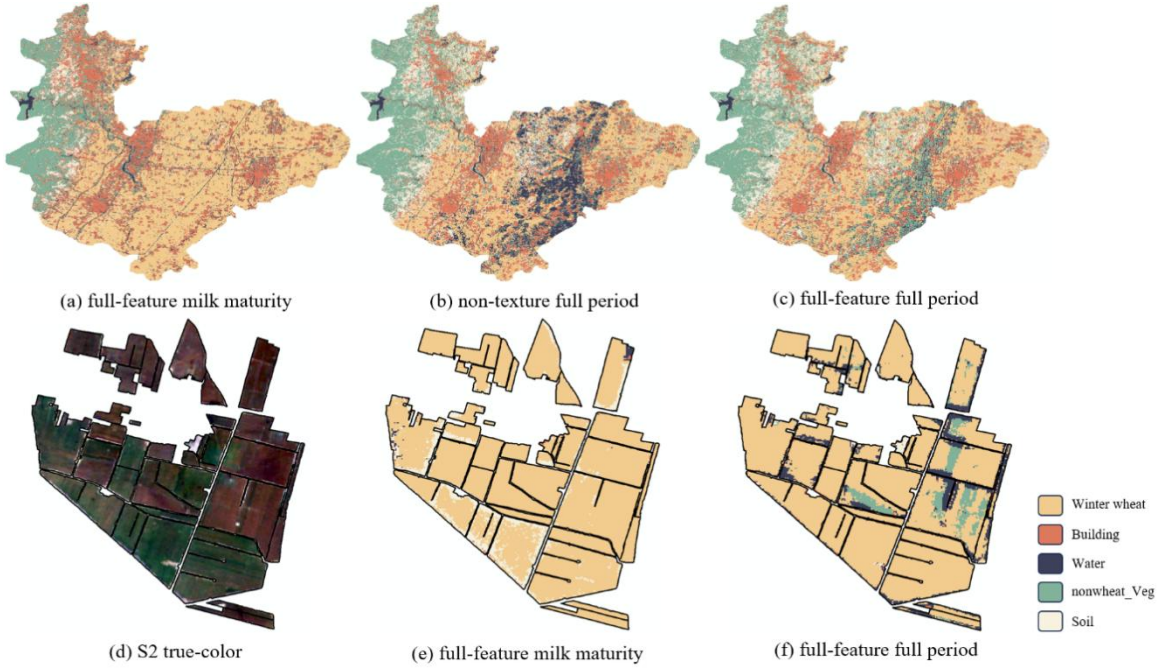

Fig. 6 Classification result plot

As shown in Figure 7, a linear fitting is made between the extracted area and the winter wheat planting area in Hebi Statistical Yearbook 2022. The R^2 of the linear fit for the entire phenological period exceeds that of the milk maturity period by 0.0022, representing less than one percent, thus indicating that the two are nearly equivalent.

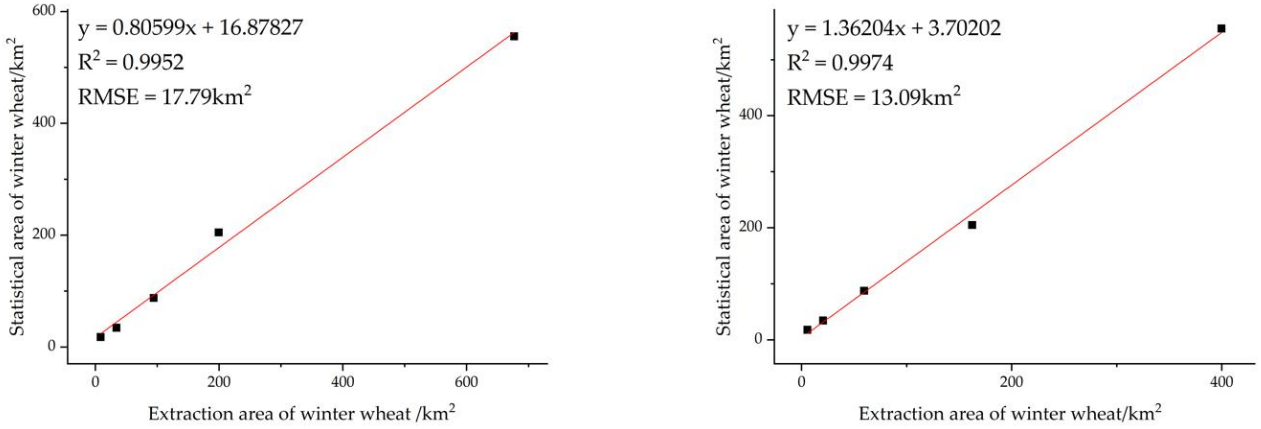

(a) full-feature milk maturity (b) full-feature full period

Fig. 7 Comparison of winter wheat planting area and extraction area in official statistics of each county

The winter wheat planting area (Table 8) was extracted from the classification results corresponding to Figure 6a and Figure 6c, respectively, and the extraction result of the full-featured milky-ripe stage was closer to the statistical yearbook data. Heshan District's agricultural pattern, characterized by minor grain crops and forestry, is shaped by the extensive barren hills and mountains of the Tai-Hang Mountains, resulting in a diverse array of cultivated crops and a complex planting structure. There are many fragmented plots of winter wheat with unclear phenological characteristics, resulting in unsatisfactory extraction results. The extraction effect in Shancheng District was the best. It belongs to the shallow hilly landform with an average altitude of 187 m. The agricultural land area accounts for 66.45% of the total, and wheat, corn, soybeans, peanuts and vegetables are mainly grown. Compared with Heshan District, the planting structure in Shancheng District is simpler, which can better extract the wheat cultivated area.

Table 8. Extraction results of winter wheat area in each county and district of Hebi City

Region	*Heshan*	*Shancheng*	*Qibin*	*Jun County*	*Qi County*	*Hebi City*
full-feature milk maturity (km^2)	8.4	34	94.1	676.8	199.3	1012.6
Proportion of area (%)	6.35	25.19	27.09	71.42	34.57	47.34
full-feature full period (km^2)	5.6	20.5	59.5	399.8	162.4	647.8
Proportion of area (%)	4.19	15.19	17.13	42.18	28.16	30.28
Statistical yearbook data (km^2)	17.9	34.5	87.7	555.6	204.9	900.6
Proportion of area (%)	12.88	17.51	25.87	57.52	36.14	40.79

3.3. Mapping of winter wheat planting distribution in Hebi City in 2021

Based on the results, the milky-ripe stage in Scheme 6 was selected as the optimal phenological period for extracting winter wheat planting information in Hebi City. Therefore, the distribution map of winter wheat planting area in 2021 was obtained (Figure 8a). We generated the slope distribution map (Figure 8b) based on the ASTER GDEM 30m DEM data obtained from the Geographic Spatial Data Cloud Platform in ARCGIS 10.8 software. According to Figure 7b, the slope

values of Heshan District, Qibin District and the west of Qi County are relatively large, which are mostly mountainous areas and not suitable for planting winter wheat. However, the planting areas of winter wheat in the central and eastern parts of Hebi City have gentler slopes mostly in the form of plains. As shown in Figure 7a, winter wheat is planted in large areas in the middle and east of Hebi, with Jun County having the widest planting range and the largest planting area, followed by Qi County, and Heshan District having the smallest winter wheat planting area, which is consistent with the results extracted from the classification results.

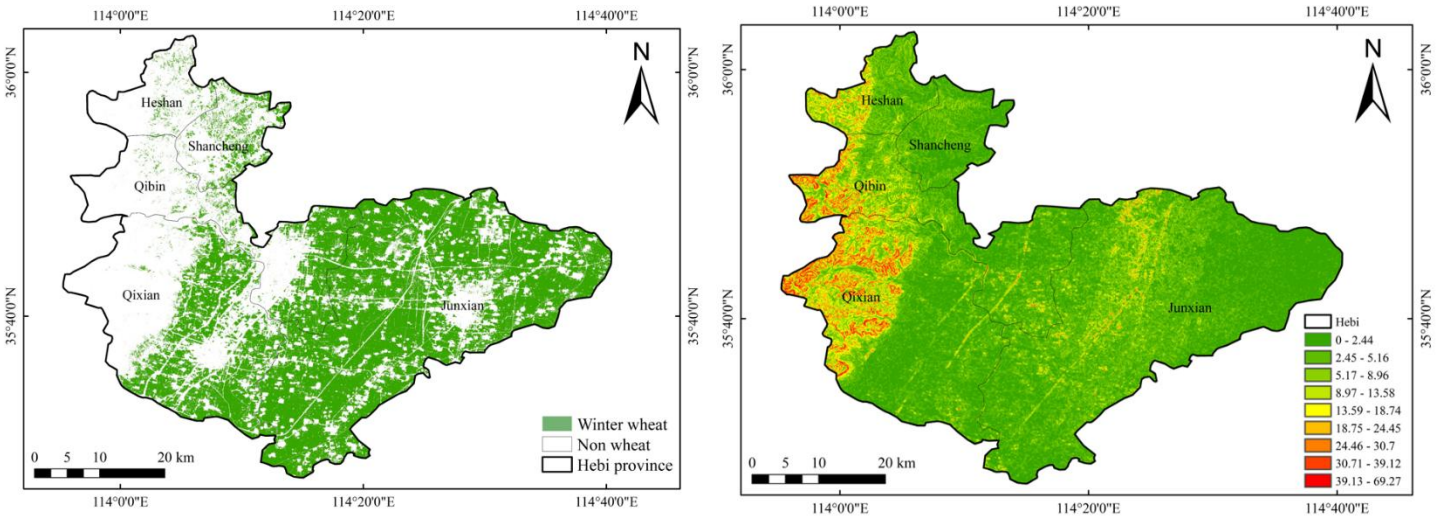

(a) Distribution map of winter wheat

(b) Slope map of Hebi City

Fig. 8 Distribution map and slope map of winter wheat in Hebi City in 2021

4. Discussion

In GEE platform and according to the NDVI change curve and actual agricultural conditions in the study area, this paper integrates Sentinel active and passive remote sensing data, and defines the whole phenological phases of winter wheat, including seedling stage, overwintering stage, green-up stage, jointing stage, heading stage, and milky stage, According to the topographic, spectral, and vegetation index feature, this paper explores the impact of texture and polarization features on area extraction accuracy (Table 9). Meanwhile, six phenological stages were identified as the control experiments with the whole phenological stage, to explore the optimal phenological stage for extracting winter wheat areas (Table 7).

Table 9. Effects of texture and polarization characteristics on winter wheat extraction

Compare plans	*2,4-1,3*	*6,8-5,7*	*5,7-1,3*	*6,8-2,4*
Feature	Texture	Texture	Polarization	Polarization
Seedling stage (%)	-5.0	-4.6	+0.5	+0.9
Overwintering period (%)	+3.8	-3.7	+3.6	-3.9
Reviving stage (%)	-3.3	0	-3.5	-0.2
Jointing stage (%)	+4.3	-3.9	+4.3	-3.9
Heading period (%)	+3.6	+0.3	+3.8	+0.5
Milk ripening period (%)	+1.0	+5.7	-4.4	+0.3
Full period (%)	+1.5	-0.2	+3.5	+5.2

During the seedling stage, the overall classification accuracy decreased when texture features were included. This may be attributed to the lack of distinct texture characteristics in winter wheat at this stage. In the overwintering and jointing stages, both texture and polarization features enhanced the accuracy of winter wheat extraction. However, combining

these two feature types led to redundancy. At the greening stage, incorporating either texture features, polarization features, or both reduced the overall accuracy from 97.2% to 93.9% and 93.7%, respectively (Table 6). This suggests that topographic, spectral, and vegetation index features alone were sufficient for distinguishing land cover types during this stage, and additional features detracted from classification accuracy. In the heading stage, adding optimized texture features or optimized polarization features individually improved extraction accuracy, while combining them provided only marginal improvement. At the milky-ripening stage, optimized texture features enhanced the overall accuracy of winter wheat extraction. Across the entire phenological period, optimized polarization features consistently improved extraction accuracy, which is consistent with the research results of Shen Yangyang (Shen et al., 2024).

The primary focus of this study was the integration of optical and radar remote sensing data. The complete phenological period was divided into six distinct phases based on the NDVI time-series curve. The most accurate phenological extraction was identified by comparing results across the entire phenological period. The study also demonstrated the effectiveness of feature optimization by excluding features with a Pearson correlation coefficient absolute value exceeding 0.8. The limitation of this study is that it concentrated solely on determining the optimal phenological period and the best extraction protocol for winter wheat, without addressing the distinction of winter wheat from other crop types within the optimal extraction period.

For future research, we will focus on two main directions. First, we aim to improve the method for distinguishing winter wheat from other crop types during optimal phenological periods. We plan to incorporate more dimensional features, such as hyperspectral characteristics and crop physiological parameters. Advanced machine learning algorithms (Zhao et al., 2022), like convolutional neural networks, will be explored to identify subtle differences in data and enhance classification accuracy. Second, we will expand the study area to test our method in regions with different climates, terrains, and more complex cropping systems. This will validate the method's adaptability and robustness. Regional-specific adjustments will be made based on local characteristics. Additionally, we plan to conduct dynamic monitoring studies. These will track winter wheat growth throughout its lifecycle and examine interactions with neighboring crops. The goal is to provide timely, comprehensive decision support for precision agriculture management.

5. Conclusion

The key findings of this study are summarized as follows:

(1) Feature optimization was performed on the 35 constructed features. The overall accuracy of all schemes exceeded 90%, demonstrating that feature optimization based on the Pearson correlation coefficient can enhance overall classification accuracy.

(2) The incorporation of polarization features improved the overall classification accuracy during the seedling, overwintering, jointing, heading, and full phenological stages, with the most significant improvement observed in the full phenological stage. The addition of texture features enhanced the overall classification accuracy during the overwintering, jointing, heading, and milky-ripening stages, particularly in the jointing stage. Moreover, the combined addition of both texture and polarization features improved the overall classification accuracy during the heading and full phenological stages, with the full phenological stage showing the most notable increase.

(3) The optimal classification scheme for extracting winter wheat planting information in Hebi is Scheme 6, which includes both preferred texture and polarization features during the milky-ripening stage. This scheme achieved an overall accuracy of 97.8% and a Kappa coefficient of 0.972.

Author Contribution

Conceptualization, methodology, X.S.; resources, project administration, funding acquisition, W.Z. and X.R.; writing—original draft and formal analysis, X.S. and X.L.; writing—review and editing, resources and supervision, Z.C. All authors have read and agreed to the published version of the manuscript.

Acknowledgements

We would like to express our sincere gratitude to all the institutions and individuals who contributed to this research. We extend special thanks to the Henan Modern Agricultural Big Data Industry Technology Research Institute Co., Ltd. for their support and for providing the agricultural survey data. The authors also would like to acknowledge the support of the PI project of Collaborative Innovation Center of Geo-Information Technology for Smart Central Plains (grant number 2023C003); the State Key Project of National Natural Science Foundation of China-Key projects of joint fund for regional innovation and development (grant number U22A20620), the State Key Project of National Natural Science Foundation of China-Key projects of joint fund for regional innovation and development (grant number U21A20108), Doctoral Science Foundation of Henan Polytechnic University (grant number B2021-20).

Conflict of Interests

The authors declare no conflicts of interest.

Data Availability

The data supporting the findings of this study are available upon request from the corresponding author.

References

Amini, S., Saber, M., Rabiei-Dastjerdi, H. and Homayouni, S., 2022, Urban land use and land cover change analysis using random forest classification of Landsat time series: *Remote. Sens,* v. 14, p. 2654, https://doi.org/10.3390/rs14112654.

Atzberger, C., and Rembold, F., 2013, Mapping the spatial distribution of winter crops at sub-pixel level using AVHRR NDVI time series and neural nets: *Remote Sensing*, v. 5, no. 3, p. 1335-1354, https://doi.org/10.3390/rs5031335.

Blickensdörfer, L., Schwieder, M., Pflugmacher, D., Nendel, C., Erasmi, S., & Hostert, P. 2022, Mapping of crop types and crop sequences with combined time series of Sentinel-1, Sentinel-2 and Landsat 8 data for Germany: *Remote sensing of environment*, v. 269, 112831, https://doi.org/10.1016/j.rse.2021.112831.

Cai, J., Luo, J., Wang, S. and Yang, S., 2018, Feature selection in machine learning: A new perspective: *Neurocomputing,* v. 300, p. 70–79, https://doi.org/10.1016/j.neucom.2017.11.077

Chang, Z., Li, H., Chen, D., Liu, Y., Zou, C., Chen, J. and Han, W., 2024, Crop identification study based on sentinel-1 and sentinel-2 for different phenological periods: *J. Anhui Norm. Univ. (Natural Sci.* v. 47, no. 1, p. 33–43, 10.14182/J.cnki.1001-2443.2024.01.005.

Chen, Y., Xi, R., Chen, J., Zhang, J., Gao, G., Liu, H., Sheng, L., Wang, F. and Liu, Z., 2024, Area extraction of winter wheat based on multi-temporal sentinel-2 satellite images: *J. Hangzhou Norm. Univ. (Natural Sci. Ed.)* v. 23, no. 02, p.209–217, 10.19926/j.cnki.issn.1674-232X.2022.12.201

Diek, S., Fornallaz, F., Schaepman, M.E. and De Jong, R., 2017, Barest pixel composite for agricultural areas using landsat time series: Remote Sensing, v. 9, no. 12, p.1245, https://doi.org/10.3390/rs9121245.

Feng, Z., Xiao, F., Lu, X., Hao, B., Wang, R. and Zhu, R., 2022, Winter wheat classification method based on feature optimization of random forest: *Bull. Surv. Mapp,* no. 3, p. 70-75, 10.13474/j.cnki.11-2246.2022.0080.

Gitelson, A.A., Kaufman, Y.J. and Merzlyak, M.N., 1996, Use of a green channel in remote sensing of global vegetation from EOS-MODIS: Remote sensing of Environment, v. 58, no. 3, pp.289-298, https://doi.org/10.1016/S0034-4257(96)00072-7.

Guo, Q., Deng, R., Wei, Y. and Xu, Z., 2021, Information extraction of rice fields in yellow river irrigation area in Yuanyang county, Henan province: *Wetl. Sci,* v. 19, no. 1, p. 40–46, 10.13248/j.cnki.wetlandsci.2021.01.004.

Hu, Q., Wu, W., Song, Q., Yu, Q., Yang, P. and Tang, H., 2015, Recent progresses in research of crop patterns mapping by using remote sensing: *Sci. Agric. Sin*, v. 48, no. 10, p. 1900–1914, 10.3864/j.issn.0578-1752.2015.10.004.

Huang, X., Huang, J., Li, X., Shen, Q. and Chen, Z., 2022, Early mapping of winter wheat in Henan province of China using time series of Sentinel-2 data: *GIScience & Remote Sensing*, v. 59, no. 1, p. 1534-1549, https://doi.org/10.1080/15481603.2022.2104999.

Huete, A.R., Liu, H.Q., Batchily, K.V. and Van Leeuwen, W.J.D.A., 1997, A comparison of vegetation indices over a global set of TM images for EOS-MODIS: Remote sensing of environment, v. 59, no. 3, pp.440-451, https://doi.org/10.1016/S0034-4257(96)00112-5.

Jakubauskas, M. E., Legates, D. R., and Kastens, J. H., 2002, Crop identification using harmonic analysis of time-series AVHRR NDVI data: *Computers and electronics in agriculture*, v. 37, no. 1-3, p.127-139, https://doi.org/10.1016/S0168-1699(02)00116-3.

Li, F., Ren, J., Wu, S., Zhao, H., and Zhang, N., 2021, Comparison of regional winter wheat mapping results from different similarity measurement indicators of NDVI time series and their optimized thresholds: *Remote Sensing*, v. 13, no. 6, p. 1162, https://doi.org/10.3390/rs13061162.

Li, X., Liu, S., Li, L., Jin, Y., Fan, W. and Wu, L., 2019, Automatic interpretation of spatial distribution of winter wheat based on random forest algorithm to optimize multi-temporal features: *Transactions Chin. Soc. for Agric. Mach,* v. 50, no. 6, p. 218–225, 10.6041/j.issn.1000-1298. 2019.06.024.

Li, X., Zhang, Y., Liu, W., Sun, R., Yin, X. and Yang, R., 2023, Extracting winter wheat information by integrating active and passive remote sensing with random forest algorithm: *J. Chifeng Univ. Sci. Ed.* V. 39, no. 10, p.44–50, 10.13398/j.cnki. issn1673-260x.2023.10.003.

Liu, M., He, W. and Zhang, H., 2024, WPS: A whole phenology-based spectral feature selection method for mapping winter crop from time-series images: *ISPRS J. Photogramm. Remote. Sen,* v. 210, p. 141–159, https://doi.org/10.1016/j.isprsjprs. 2024.03.005.

Liu, S., Peng, D., Zhang, B., Chen, Z., Yu, L., Chen, J., Pan, Y., Zheng, S., Hu, J., Lou, Z., Chen, Y. and Yang, S., 2022, The accuracy of winter wheat identification at different growth stages using remote sensing: *Remote Sensing*, v.14, no. 4, p. 893, https://doi.org/10.3390/rs14040893.

Liu, W. and Ma, J., 2022, Extraction of winter wheat planting area of fusion on phenological knowledge and multi temporal remote sensing. Mod: *Inf. Technol,* v. 6, no. 06, p. 141–143+147, 10.19850/j.cnki.2096-4706.2022.06.036.

Lucas, R., Van De Kerchove, R., Otero, V., Lagomasino, D., Fatoyinbo, L., Omar, H., Satyanarayana, B. and Dahdouh-Guebas, F, 2020, Structural characterization of mangrove forests achieved through combining multiple sources of remote sensing data: *Remote Sensing of Environment*, v. 237, 111543, https://doi.org/10.1016/j.rse.2019.111543.

Luo, H., Li, M., Dai, S., Li, H., Li, Y., Hu, Y., Zheng, Q., Yu, X. and Fang, J., 2022, Combinations of feature selection and machine learning algorithms for object-oriented betel palms and mango plantations classification based on Gaofen-2 imagery: *Remote Sensing*, v. 14, no. 7, p. 1757, https://doi.org/10.3390/rs14071757.

Luo, H., Li, W., Jing, Y., Xu, X. and Chen, H., 2019, Remote sensing extraction of winter wheat planting area based on svm: *J. Triticeae,* v. 39, no. 4, p. 455–462, 10.7606/j.issn.1009-1041.2019.04.11.

Ma, Z., Liu, C., Xue, H., Li, J., Fang, X. and Zhou, J., 2021, Identification of winter wheat by integrating active and passive remote sensing databased on google earth engine platform: *J. Chifeng Univ. Sci. Ed.* V. 52, no. 09, p.195–205, 10.6041/j.issn.1000-1298.2021.09.023.

Mashonganyika, F., Mugiyo, H., Svotwa, E. and Kutywayo, D., 2021, Mapping of winter wheat using sentinel-2 NDVI data. a case of Mashonaland central province in Zimbabwe: *Frontiers in Climate*, v. 3, p.715837, https://doi.org/10.3389/fclim.2021.715837.

Nguyen, C. T., Chidthaisong, A., Kieu Diem, P. and Huo, L.-Z., 2021, A Modified Bare Soil Index to Identify Bare Land Features during Agricultural Fallow-Period in Southeast Asia Using Landsat 8: Land, v. 10, no. 3, p. 231, https://doi.org/10.3390/land10030231.

Pan, Y., Li, L., Zhang, J., Liang, S. and Hou, D., 2011, Crop area estimation based on MODIS-EVI time series according to distinct characteristics of key phenology phases: A case study of winter wheat area estimation in small-scale area: *J. Remote. Sens.* v. 15, no. 3, p. 578–594, 10.11834/jrs.20110066.

Potgieter, A.B., Apan, A., Dunn, P. and Hammer, G., 2007, Estimating crop area using seasonal time series of Enhanced Vegetation Index from MODIS satellite imagery: *Australian Journal of Agricultural Research*, v. 58, no. 4, p. 316-325, https://doi.org/10.1071/AR06279.

Praticò, S., Solano, F., Di Fazio, S. and Modica, G., 2021, Machine learning classification of mediterranean forest habitats in google earth engine based on seasonal sentinel-2 time-series and input image composition optimization: Remote Sensing, v. 13, no. 4, p. 586:1-28, https://doi.org/10.3390/rs13040586.

Pu, D., Wang, G., Zhang, Z., Niu, X., He, G., Long, T., Yin, R., Jiang, W. and Sun, J., 2020, Urban area extraction based on independent component analysis and random forest algorithm: *J. Geo Inf. Sci,* v. 22, no. 8, p. 1597–1606, DOI:10.12082/dqxxkx.2020.190385

Qi, J., Chehbouni, A., Huete, A.R., Kerr, Y.H. and Sorooshian, S., 1994, A modified soil adjusted vegetation index: Remote sensing of environment, v. 48, no. 2, pp.119-126, https://doi.org/10.1016/0034-4257(94)90134-1.

Qi, X., Sun, D. and Jia, L., 2022, Crop classification and monitoring of sentinel 2 multi temporal vegetation index; *Eng. Surv. Mapp.* v. 31, no. 6, p. 47–53, 10.19349/j.cnki.issn1006-7949.2022.06.008.

Qu, C., Li, P. and Zhang, C. A spectral index for winter wheat mapping using multi-temporal Landsat NDVI data of key growth stages: *ISPRS J. Photogramm. Remote. Sens.* v. 175, p. 431–447, https://doi.org/10.1016/j.isprsjprs.2021.03.015.

Radočaj, D., Šiljeg, A., Marinović, R. and Jurišić, M., 2023, State of major vegetation indices in precision agriculture studies indexed in web of science: A review: *Agriculture,* v. 13, no. 3, p. 707, https://doi.org/10.3390/agriculture13030707 .

Ren, S., Guo, B., Wu, X., Zhang, L., Ji, M., and Wang, J., 2021, Winter wheat planted area monitoring and yield modeling using MODIS data in the Huang-Huai-Hai Plain, China: *Computers and Electronics in Agriculture*, v. 182, 106049, https://doi.org/10.1016/j.compag.2021.106049.

Rondeaux, G., Steven, M. and Baret, F., 1996, Optimization of soil-adjusted vegetation indices: Remote sensing of environment, v. 55, no. 2, pp.95-107, https://doi.org/10.1016/0034-4257(95)00186-7.

Rouse Jr, J.W., Haas, R., Schell, J.A. and Deering, DW., 1973, Monitoring vegetation systems in the Great Plains with ERTS: In Earth resources technology satellite-1 symposium, v. 3, p. 307â, https://ntrs.nasa.gov/citations/19740022614.

Schlund, M. and Erasmi, S., 2020, Sentinel-1 time series data for monitoring the phenology of winter wheat: *Remote Sensing of Environment*, v. 246, p. 111814, https://doi.org/10.1016/j.rse.2020.111814.

Sun, C., Tao, Y., Liu, S., Wang, S., Xu, H., Shen, Q., Li, M. and Yu, H., 2024, Automatic mapping of winter wheat planting structure and phenological phases using time-series sentinel data: *Scientific Reports*, v. 14, no. 1, p. 17886. https://doi.org/10.1038/s41598-024-68960-0

Shen, Y., Feng, S., Xu, X., Liu, L., Yan, Z., Wu, J. and He, H., 2024, Research on extraction of winter wheat planting area using collaborative active and passive remote sensing technology: Natural Resources Informatization, no. 0, p. 1-10, https://link.cnki.net/urlid/10.1797.n.20241227.1547.004

Tian, X., Zhang, Y., Liu, R. and Wei, J., 2022, Winter wheat planting area extraction over wide area using vegetation red edge information of multi-temporal Sentinel-2 images: *National Remote Sensing Bulletin*, v. 26, no. 10, p. 1988-2000, 10.11834/jrs.20211359.

Uddin, M., Mamun, M. and Hossain, M., 2021, PCA-based feature reduction for hyperspectral remote sensing image classification: *IETE Tech. Rev,* v. 38, no. 4, p. 377–396, https://doi.org/10.1080/02564602.2020.1740615.

Wang, F., Li, J., Duan, S., Yu, Q., Ye, S., Xu, T. and Shi, Z., 2023, New demands and challenges for the development of agricultural remote sensing: *China Agric. Informatics,* v. 35, no. 06, p. 9–21, 10.12105/j.issn.1672-0423.20230602.

Wang, M., Wang, L., Guo, Y., Cui, Y., Liu, J., Chen, L., Wang, T. and Li, H., 2024. A Comprehensive Evaluation of Dual-Polarimetric Sentinel-1 SAR Data for Monitoring Key Phenological Stages of Winter Wheat: *Remote Sensing*, v. 16, no. 10, p. 1659, https://doi.org/10.3390/rs16101659.

Wang, Y., Yang, D., Dong, G., Chen, J. and Yang, T., 2023, Extraction of winter wheat planting area in zhong mu county based on multi-temporal sentinel-2 data: *Henan Sci.* v. 41, no. 09, p. 1285–1291, 10.3969/j.issn.1004-3918.2023.09.006.

Wu, X., Hua, S., Zhang, S., Gu, L., Ma, C. and Li, C., 2023, Extraction of winter wheat distribution information based on multi-phenological feature indices derived from sentinel-2 data: *Transactions Chin. Soc. for Agric. Mach,* v. 54, no. 12, p. 207–216, http://kns.cnki.net/kcms/detail/11.1964. s.20241010.1626.008.html

Xiao, X., Jiang, L., Liu, Y. and Ren, G., 2023, Limited-Samples-Based Crop Classification Using a Time-Weighted Dynamic Time Warping Method, Sentinel-1 Imagery, and Google Earth Engine: *Remote Sensing*, v. 15, no. 4, p. 1112, https://doi.org/10.3390/rs15041112.

Xie, Y., Wang, J. and Liu, Y., 2024, Research on winter wheat planting area identification method based on sentinel-1/2 data feature optimization: *Nongye Jixie Xuebao/Transactions Chin. Soc. Agric. Mach.* v. 55, no. 2, p. 231-241, https://link.cnki.net/urlid/11.1964.S.20231215.1557.003.

Xiong, H., Zhou, X., Wang, X. and Cui, Y., 2021, Mapping the spatial distribution of tea plantations with 10 m resolution in fujian province using google earth engine: *J. Geo-Inf. Sci,* v. 23, no. 7, p. 1325–1337, 10.12082/dqxxkx.2021.200583.

Xu, H., 2005, A Study on Information Extraction of Water Body with the Modified Normalized Difference Water Index (MNDWI): Journal of Remote Sensing, no. 5, p. 589-595, 10.11834/jrs.20050586.

Yan, F., Wang, Y., Wu, J., and Li, C., 2009, Extracting winter wheat area using temporal sequence of Ts-EVI: *Transactions of the Chinese Society of Agricultural Engineering*, v. 25, no. 4, p.135-140, http://www.tcsae.org//article/id/20090426.

Yang, H., Wang, Z., Bai, J. and Han, H., 2020, Winter wheat area extraction based on multi-feature extraction and feature selection: *J. Shaanxi Norm. Univ. (Natural Sci. Ed.),* v. 48, no. 01, p. 40–49, 10.15983/j.cnki.jsnu.2020.04.005.

Yao, J., Wang, L., Li, J., Zhang, K. and Zhang, Z., 2022, Multi-source remote sensing and multi-feature combination ground object classification in nuomuhong areas, qinghai province of China: Transactions Chin. *Soc. Agric. Eng. (Transactions CSAE),* v. 38, no. 3, p. 247–256, 10.11975/j.issn.1002-6819.2022.03.029.

Zha, Y., Ni, S. and Yang, S., 2003, An Effective Approach to Automatically Extract Urban Land-use from TM lmagery: Journal of Remote Sensing, no. 1, pp. 37-40, 10.11834/jrs.20030107.

Zhang, H., Zhang, Y., Tian, Z., Wu, J., Li, M. and Liu, K., 2023, Extraction of planting structure of winter wheat using GBDT and google earth engine: *SPECTROSCOPY AND SPECTRAL ANALYSIS,* v. 43, no. 2, p. 597–607, 10.3964/j.issn.1000-0593(2023)02-0597-11

Zhang, K., Cheng, G., Wu, W., Song, X., Zhang, Z., Yao, S. and Wu, S., 2023, Extraction of winter wheat planting area based on fused active and passive remote sensing images: *J. Henan Agric. Sci.* v. 52, no. 06, p. 160–171, 10.15933/j.cnki.1004-3268.2023.06.017.

Zhang, Q., Wang, G., Wang, G., Song, W., Wei, X., and Hu, Y., 2023, Identifying Winter Wheat Using Landsat Data Based on Deep Learning Algorithms in the North China Plain: *Remote Sensing*, v. 15, no. 21, p. 5121, https://doi.org/10.3390/rs15215121.

Zhang, X. W., Liu, J. F., Qin, Z., & Qin, F, 2019, Winter wheat identification by integrating spectral and temporal information derived from multi-resolution remote sensing data: *Journal of Integrative Agriculture*, v. 18, no. 11, p. 2628-2643, https://doi.org/10.1016/S2095-3119(19)62615-8.

Zhao, J., Zhan, Y., Wang, J. and Huang, L., 2022, Se—UNet-based extraction of winter wheat planting areas: *Transactions Chin. Soc. for Agric. Mach*, v. 53, no. 9, p. 189–196, 10.6041/j.issn.1000-1298.2022.09.019.

Zhao, Y. and Zhu, Z., 2022, ASI: An artificial surface Index for Landsat 8 imagery: International Journal of Applied Earth Observation and Geoinformation, v. 107, p. 102703, https://doi.org/10.1016/j.jag.2022.102703.

Zhao, Y., Wang, X., Hou, X. and Zhang, A., 2021, Spatio-temporal characteristics of key phenology of winter wheat in shandong province from 2003 to 2019: *Acta Ecol. Sinica,* v. 41, no. 19, p. 7785–7795, 10.5846/stxb202011132937